This is a peer-reviewed, accepted author manuscript of the following article: Tauanov, Z., Lee, J., & Inglezakis, V. J. (2020). Mercury reduction and chemisorption on the surface of synthetic zeolite silver nanocomposites: equilibrium studies and mechanisms. *Journal of Molecular Liquids*, *305*, [112825]. https://doi.org/10.1016/j.molliq.2020.112825

Graphical abstract

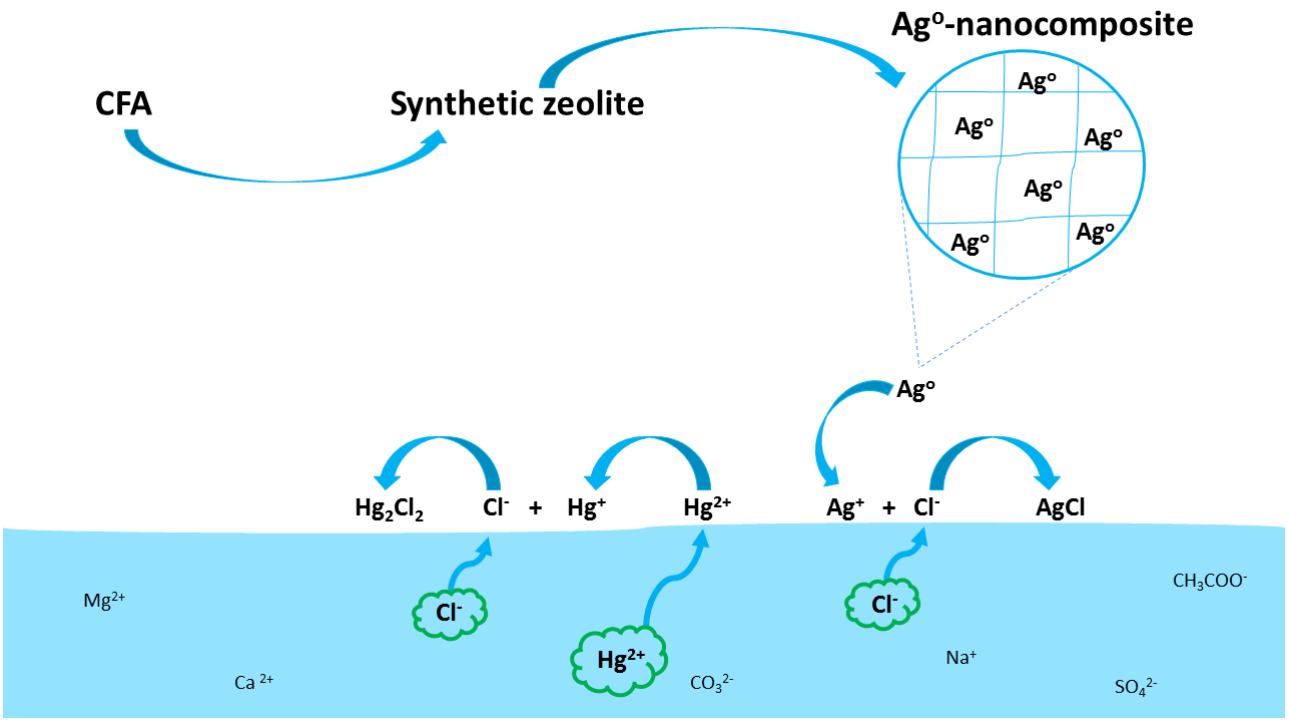

Highlights:

- Synthesis of coal fly ash derived silver-doped zeolitic nanocomposites
- The adsorption capacity of the zeolite increased by 5 times after the impregnation of Ag
- Adsorption isotherms of novel silver-doped zeolitic nanocomposites
- Surface redox reaction between Ag^{o} and Hg^{2+} and subsequent formation of calomel

Mercury reduction and chemisorption on the surface of synthetic zeolite silver nanocomposites: Equilibrium studies and mechanisms

Z. Tauanov[1,2], J. Lee[2] and V.J. Inglezakis[1,3]

[1] Environmental Science and Technology Group (ESTg), Chemical and Materials Engineering Department, School of Engineering and Digital Sciences, Nazarbayev University, Nur-Sultan, 010000, Kazakhstan

[2] Department of Chemistry, Chungnam National University, Daejeon, 34134, Republic of Korea

[3] The Environment and Resource Efficiency Cluster (EREC), Nazarbayev University, Nur-Sultan, 010000, Kazakhstan

Corresponding author: vasileios.inglezakis@nu.edu.kz

Abstract

This work presents the utilization of a coal power plants waste, namely coal fly ash for the synthesis of synthetic zeolites and silver nanocomposites for the removal of Hg^{2+} from water. Equilibrium data are derived for all materials for mercury concentration range of 10-500 mg/L and models are applied. The removal mechanisms are discussed in detail and complemented by XRD, XRF, SEM-EDS, and TEM characterizations and water phase mercury speciation modeling. According to findings, the adsorption capacity of zeolites is about 4 mg/g, increased by almost 5 times after the modification with silver nanoparticles to 20.5-22.3 mg/g. Langmuir equilibrium model fits well the experimental data for the nanocomposites indicating monolayer adsorption process. The mechanism complex, involving Hg^{2+} reduction to Hg^{+} and possibly Hg^{0} followed by formation of calomel and amalgams on the surface of the nanocomposites. The mercury reduction is accompanied by Ag^{0} oxidation to Ag^{+} and subsequent formation of silver chloride.

Keywords: Zeolites; nanocomposites; silver; mercury removal; adsorption isotherms.

1. Introduction

Mercury is one of the most toxic and hazardous heavy metals found in nature. It is commonly used in many industries, such as electronics, paper, and pulp manufacturing, metallurgy, polymers production, pharmaceutical, oil refinery and others [1,2]. The worst scenario of the waste mercury generation is that after being used it is usually discharged to water resources. Mercury could exist in three oxidation states, +1 as in HgCl, +2 as in $HgCl_2$ and +4 as in HgF_4, the latter state is identified in exceptional conditions [3]. The widely spread compound form of this metal is mercury (II) chloride that is typically used in polyvinyl chloride production and exists as Hg^{2+} form in the aqueous environment. Mercury might also bind with organic compounds, as in highly toxic methylmercury (CH_3Hg). One of the unique and unfortunately negative sites of Hg is the capability of volatilization, persistence, and bioaccumulation in food products, animals and human body.

According to literature, more than 100 000 kg of Hg was produced due to human activities and discharge from various industries, annually [3]. The power stations that mostly use different types of coal has hugely contributed to the current total Hg emissions [3]. Both gaseous and aqueous phase Hg have mainly produced from these coal-fired power plants [4]. The recent studies on Hg contamination report that all forms of Hg, including the metallic mercury (Hg^0), the ionic form of mercury (Hg^{2+}) and organic mercury (CH_3Hg), have made their way to the environment and human health [5]. Currently, the pollution with Hg and its species is widely spread and could be detected in water resources, rocks, soil and even in air [6,7]. In 2013, the Minamata convention was signed to preserve the human health and environment from anthropogenic release and lifecycle of mercury in atmosphere, water and soil [8,9]. Therefore, researchers from all over the world are trying to resolve this issue and find the solution of efficient remediation of Hg from water and flue

gas. There are several existing purification approaches that are typically applied for removal of Hg^{2+} from aqueous media, particularly removal via physical and chemical adsorption.

One of the efficient ways of Hg removal is by applying adsorption methods due to its convenience and practicality amongst current separation technologies and there are several materials that have been used for the removal of mercury from water [10]. Coal fly ash (CFA) is a waste produced in large amounts in power plants and there is a lot of interest in its utilization, one the most promising being the synthesis of zeolites [11,12]. However, there are limited studies on the removal of mercury from water by use of CFA-derived zeolites, as for instance this of Attari *et al*. [13] and only few on their silver forms, these of Czarna *et al*. [14] who used ion exchanged Ag-zeolites and Tauanov *et al*. [15,16] who used Ag^0-zeolites. In the work of Czarna *et al*. no reduction was done and although the XRD shows Ag^0 peaks most probably the majority of silver was in ion form as the results showed that the modification had no effect on the Hg removal. On the other hand, Tauanov *et al*. did reduction and the silver is metallic and the modified forms had a considerable effect on Hg removal. However, these were kinetics and not equilibrium studies and is well known that in order to better understand the behavior of the adsorbent the study of the equilibrium is necessary.

Based on the above and to the best of our knowledge there is no equilibrium study on Hg adsorption by Ag^0-CFA nanocomposites. Furthermore, there is a lack of comprehensive studies on the mechanisms of Hg-Ag interaction on solid surfaces. In the present study we extend the research on the removal of Hg by Ag^0-CFA nanocomposites by presenting equilibrium isotherms and discussing in detail the Hg-Ag interaction and removal mechanisms.

2. Materials and methods

2.1. Materials

The coal fly ash samples (Karazhyra and Maikuben CFAs) employed in the research were collected from electrostatic precipitators of Oskemen city power plant (East Kazakhstan, 252 MW). Sodium hydroxide pearls (NaOH, 98%, Sigma-Aldrich, UK) were used for a hydrothermal alkaline treatment of coal fly ash into synthetic zeolites. Silver nitrate powders (AgNO3, 99%, Sigma-Aldrich, UK) were used for silver io exchange and subsequent reduction to nanoparticles. Sodium borohydride (NaBH4, 98%, Sigma-Aldrich, UK) was used for the reduction of silver ions into silver nanoparticles on the surface of nanocomposites. The concentrated solution of nitric acid (HNO_3, Sigma-Aldrich, UK) was used to adjust the pH of the solutions. The chemical reagents used in the synthesis of nanocomposites were of analytical grade and used prior to experiments.

2.2. Synthesis of zeolite

Coal fly ash derived synthetic zeolites were synthesized via hydrothermal alkaline treatment. First, carefully weighed 50 g of CFA samples were placed into 1-liter heavy-walled reactor. Then the freshly prepared 3M aqueous solution of NaOH was poured into the reactor that was used as an activation agent. The reactor was connected to cooling system and a laboratory thermometer was installed to control the reaction temperature during the synthesis. The mixture of CFA and NaOH was vigorously stirred under constant rate of 125 rpm with an incubation reaction time of 48 hours. After the hydrothermal alkaline treatment the crude products were filtered using laboratory filter papers and thoroughly purified using excess amount of deionized water. The qualitative monitoring of any remaining NaOH was performed using indictor papers and continued until it reached the pH of 6.5-7.0. The final products were fully dried in a laboratory oven under 70^{o}C over 12 hours and the synthetic zeolites (ZFAs) were stored in a tightly closed container.

2.3. Synthesis of nanocomposite

The freshly produced ZFAs were impregnated with silver nanoparticles (Ag NPs) via ion-exchange and reduction reactions in order to use these novel nanocomposites for mercury remediation from water. In the beginning, ZFA samples were fully dried at 300^{o}C for 3 hours to remove any remaining moisture within the structure of materials. Then, a conventional ion-exchange reaction was conducted by adding 10 mL of 10 mM aqueous solution of $AgNO_3$ (Sigma-Aldrich) per 1 g of zeolite and left to cure for 12 hours. The reaction container was covered with aluminium foil and stored in dark place to prevent oxidation of silver ions. Finally, the ion-exchanged ZFAs slurry were dried at 130^{o}C for 3 hours. The same soaking procedure was repeated twice to produce silver ion-exchanged zeolites (Ag^{+}-ZFA) with approximately 2wt.% Ag NPs. The obtained Ag^{+}-ZFA was then annealed for 3 hours at 500^{o}C, followed by 4 hours of silver ions reduction using $NaBH_4$ (Fischer-Scientific) as the reducing agent, thus producing nanocomposites with various Ag NPs loadings (Ag-ZFA). The freshly produced nanocomposites were labeled as Ag-K-ZFA (Karazhyra) and Ag-M-ZFA (Maikuben), which corresponds to the raw CFA used for synthesis. The detailed experimental procedure of zeolite and nanocomposite synthesis can be found elsewhere [15,17–19].

2.4. Characterization of materials

Chemical analysis of Ag-ZFAs were conducted using standardless X-Ray fluorescence (XRF, PANalytical) spectrometer under helium atmosphere in a powder sample mode. The mineralogical composition was identified on X-Ray diffraction (XRD, Rigaku) using Rigaku SmartLab diffraction system with CuKβ radiation at 40 kV and 30 mA. The morphological characteristics of zeolites were studied by Scanning Electron Microscopy (SEM) using a JEOL 6380LV Scanning Electron Microscope, operating in LV mode, at 20KV, equipped with a backscattered electron detector. Spot and area analyses were carried out using a Si(Li) Energy-Dispersive X-ray spectrometer (INCA X-sight, Oxford Instruments), connected to SEM. The nanoscale investigation was performed with

a high resolution JEOL JEM-2100 LaB_6 transmission electron microscope (HR-TEM), operating at 200 kV. The elemental analysis was carried out using an Oxford X-Max 100 Silicon Drift Energy Dispersive X-ray spectrometer connected to TEM, with a probe size ranging from 2 to 5 nm.

2.5. Batch adsorption equilibrium

Adsorption equilibrium isotherms were performed in 40 mL solution of $HgCl_2$ with starting concentrations of 10-550 mg/L and dosage of 0.2 g adsorbent. The initial pH of solutions were adjusted to 2 using concentrated nitric acid, whereas the final pH of solutions was around 6.25. The experiments were carried out at room temperature and static conditions. The aliquots volume of 50-100 µL were taken from adsorption containers to measure the residual concentrations on MA until equilibrium attained. The amount of mercury removed was calculated from the difference between the initial and residual concentrations:

$$q_{eq} = \frac{C_o - C_f}{m} \times V \quad (1)$$

where, q_{eq} is the Hg loading on the material (mg/g), C_o and C_f are Hg concentrations (mg/L) in the initial and final solutions, respectively, V the volume of solution (L), and m is the initial weight of the zeolite (g). To avoid confusion, throughout the paper the term “loading” and symbol q (mg/g) is used for the amount of species adsorbed per initial weight of the solid phase (before adsorption) and the term “content” and symbol ct (mg/g) for the amount of species adsorbed per total weight of the solid phase (initial weight plus the weight of the adsorbed species). The former is typically used for kinetics and equilibrium studies while the later for XRF, EDS and other compositional analyses and they are related as follows:

$$ct = \frac{q}{1 + \left(\frac{q}{1000}\right)} \quad (2)$$

The experiments were conducted in duplication and the average values are presented. Two blanks were used; one with the same initial concentration of mercury and volume without solids and the second with deionized water with solids. Blank experiments showed that the Hg losses due to adsorption on container walls are limited to an average of 6.5%. All experiments were carried out in duplicate and the average standard deviation was below 1.5%.

3. Results and discussion

3.1. Characterization

The mineralogical composition of silver nanoparticles containing composites were thoroughly analyzed on XRD. According to analysis, the two nanocomposites derived from corresponding CFA-based synthetic zeolites contain sodalite (Ag-M-ZFA) and analcime (Ag-K-ZFA) as major phases, which are produced due to alkaline hydrothermal treatment of parent CFAs.

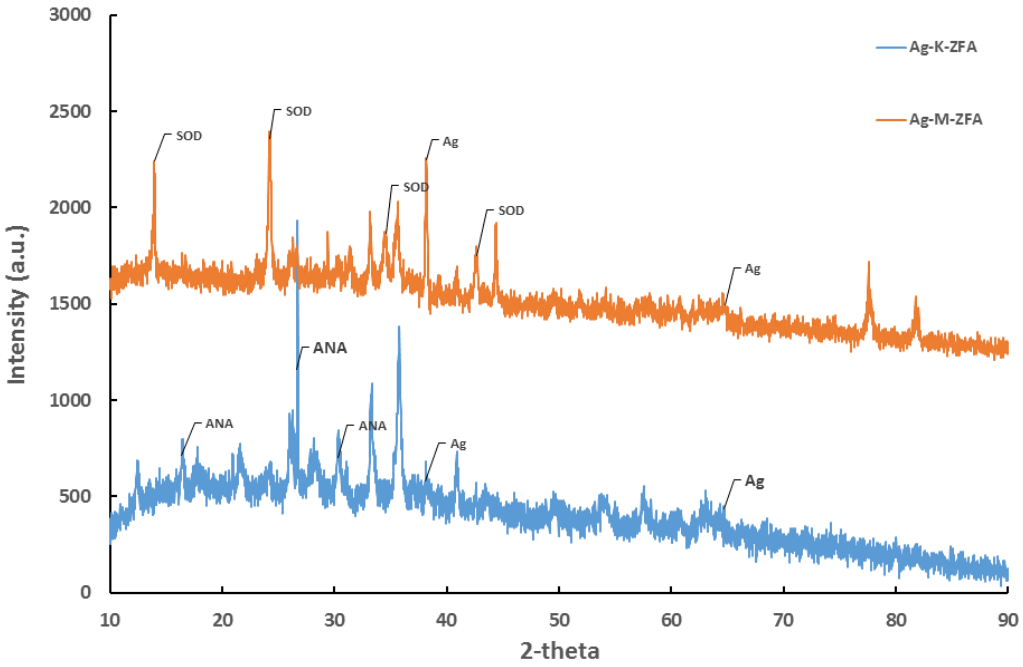

Fig. 1. XRD spectra of pristine nanocomposites (SOD: Sodalite; ANA: Analcime; Ag: silver NPs)

The post-modification of both synthetic zeolites to produce Ag-ZFA nanocomposites have also been confirmed by the distinctive peaks of Ag NPs phases at 38.18° and 64.52° in matrix as depicted in Fig. 1. The morphology of zeolites, on the other hand, was studied on SEM as shown in Fig. 2. The microstructural images demonstrate a growth of zeolitic phases in both adsorbents that possess a crystalline structure. It should be noted that the raw CFAs contain phases that are non-transformable (usually with undistinctive shape and size) into zeolitic phase, which in turn might be seen on morphological analysis as side fractions. The chemical composition of Ag-ZFAs also confirm the presence of major expected fractions as SiO_2 and Al_2O_3, whcih in total comprise approximately 35wt.%. The formation of Ag NPs after impregnation via ion-exchange followed by reduction reveals a close to theoretical amount (2.15wt.%) in both nanocomposites (2.25wt% and 2.33wt.% in Ag-M-ZFA and Ag-K-ZFA, respectively) that validates an efficient impregnation. Further data on mineralogy, morphology and chemical composition of parent CFAs, synthesized zeolites and nanocomposites can be found elsewhere [16,18,19].

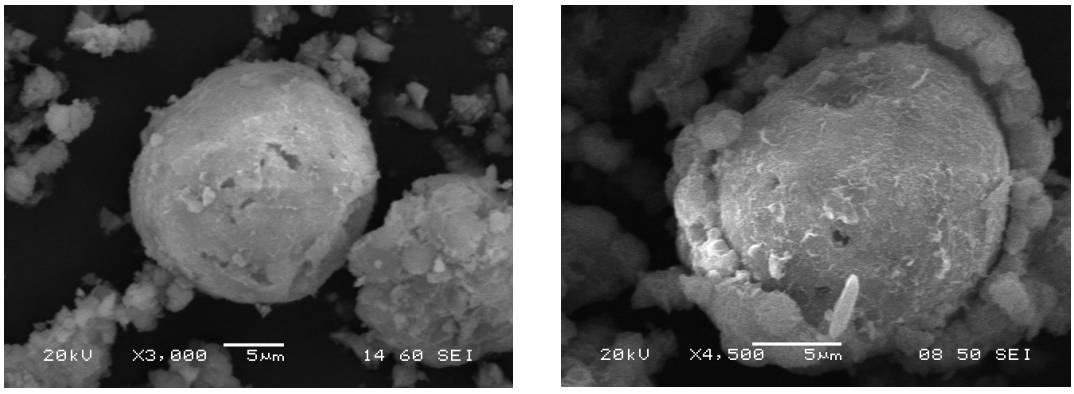

K-ZFA **M-ZFA**

Fig. 2. SEM images of the zeolite crystal growth on the CFA particles

The presence of Ag NPs and the particle distribution range has also been analyzed on TEM micrographs (Fig. 3). The results reveal that the nanoparticles are relatively homogenously distributed within the matrix of zeolites with particle size ranging from 5-45 nm in both samples.

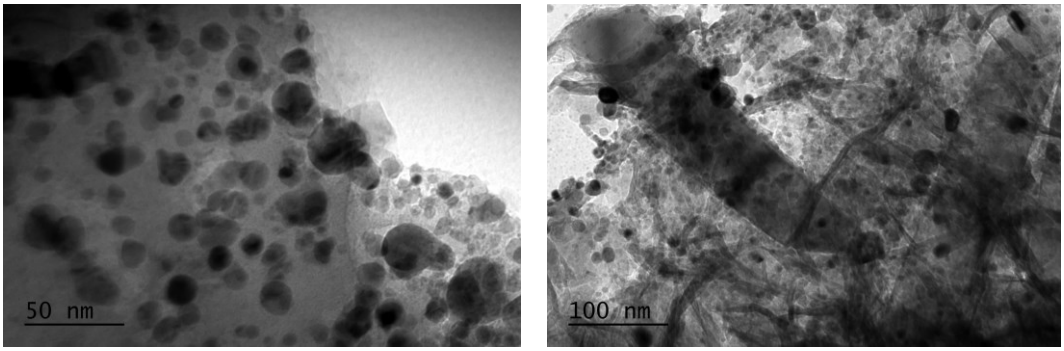

Ag-K-ZFA **Ag-M-ZFA**

Fig. 3. TEM analysis of as produced nanocomposites

The BET surface areas of nanocomposites show a relatively similar values at 34 m^2/g and 51 m^2/g for Ag-K-ZFA and Ag-M-ZFA, respectively [15]. The average pore size, on the one hand, reveals to range between 10-15 nm for Ag-ZFAs with the pore volumes of 0.13-0.22 cm^3/g. The particle size distribution analysis of both nanocomposites Ag-K-ZFA and Ag-M-ZFA were 9.53 ± 4.02 µm and 20.43 ± 0.04 µm, respectively [15]. The pore size distribution of both Ag-ZFAs demonstrate a mesoporous structure with a comparable surface area. It should be emphasized that the radii size of ionic mercury with +2 charge is around 0.1 nm, which is suitable to be entrapped within the microstructure of nanocomposites.

3.2. Adsorption equilibrium isotherms

The adsorption equilibrium of zeolites and nanocomposites are shown in Fig. 4 and 5. The shape of isotherms suggests a reversible phenomenon. According to results, the ZFAs (have the maximum adsorption capacity of about 4 mg/g, while the corresponding nanocomposites reveal much higher removal profiles at 20.5-22.3 mg/g (Ag-K-ZFA and Ag-M-ZFA). These entails that the adsorption behavior is inherently diverse than in parent zeolites as hypothesized. Also, the adsorption capacity values are higher than in CFA-zeolites used for mercury removal in literature [13], which

210 further confirms the enhancement of adsorption properties due to silver impregnation into zeolitic

211 matrix.

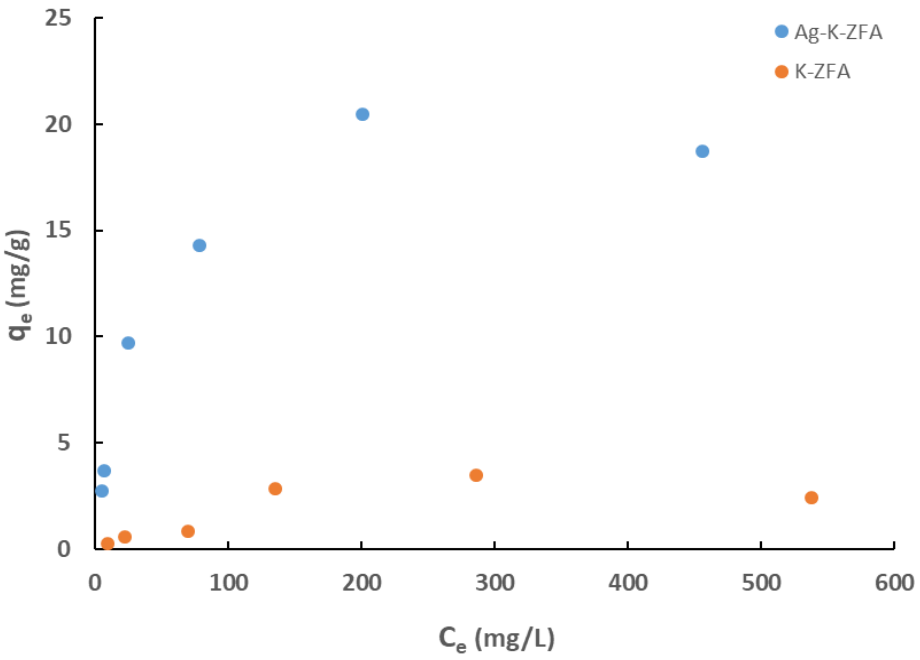

212

213 **Fig. 4.** The adsorption equilibrium isotherms of K-ZFA and Ag-K-ZFA

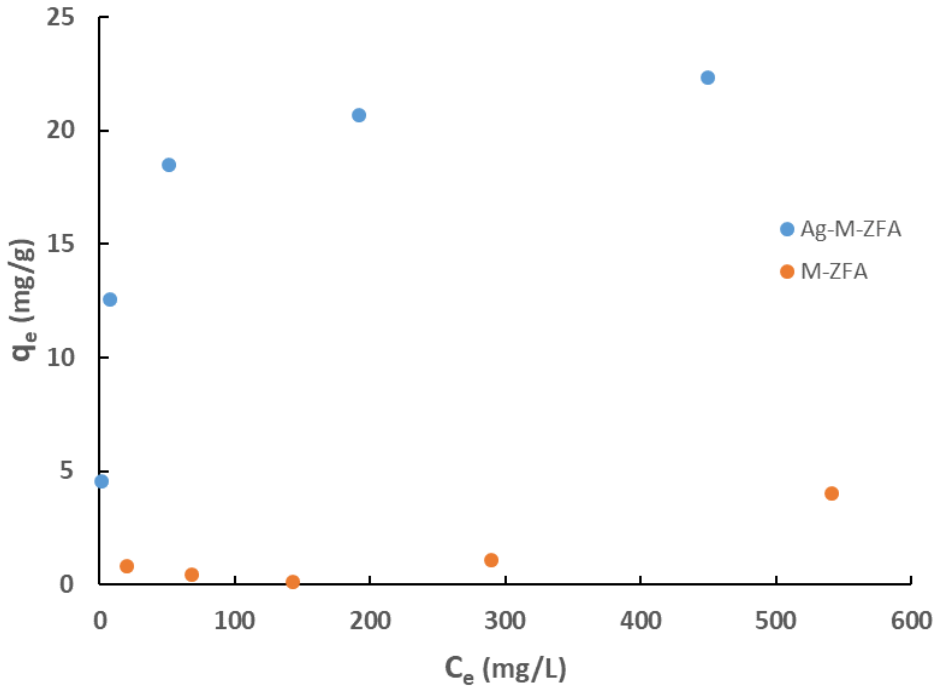

214

215 **Fig. 5.** The adsorption equilibrium isotherms of M-ZFA and Ag-M-ZFA

216

217 Czarna *et al*. measured a similar maximum capacity close to 5 mg/g for the CFA-zeolites but

218 observed no effect of the Ag impregnation. This is probably due to the fact that no reduction was

done and although the XRD shows Ag^0 peaks most probably the majority of silver was in Ag^+ form, which is inactive towards Hg^{2+}. A comparative summary of adsorption equilibrium studies in literature with applied isotherm models is presented in Table 1.

Table 1. Equilibrium studies on Hg^{2+} removal from water

Adsorbent type	Adsorption capacity [mg/g]	pH range	Initial concentration [mg/L]	Isotherm models*	Ref.
CFA-derived Ag^o-nanocomposite	20.5-22.3	2.0	10-550	L, F	This work
CFA- derived zeolite	0.3	2.5	10	L, F, T	[13]
CFA- derived zeolite	5.10	5-6	13.2-575	L, F, T	[14]
Ag-doped CFA- derived zeolite	5.04	5-6	13.2-575	L, F, T	[14]
Deep eutectic solvent functionalized carbon nanotubes	24	6.5	70	L, F	[20]
Ternary hydro-sulphonyl based deep eutectic solvent modified magnetic graphene oxide	215	3.0-10	60	L, F	[21]
Pistachio wood derived activated carbon	202	7.0	45	L, F, T, DR, RP, S, T	[22]
Fe2O3@SiO2 thin films	126	7.0	335.8	L, F, T, RP, BS	[23]
Bacillus thuringiensis MC28	74	2-8	100	L, F, T, DR, RP, S, TH	[24]
Sulfurized wood biochar	108	6.0	320	L, F	[25]
d-MoS_2 nanosheets with Fe_3O_4 nanoparticles	426	5.0	200	L, F	[26]
Alkynyl carbon materials	192	5.8	50	L, F	[27]
Polyaniline nanoparticles on the polyurethane foam	15	7.0	27.5	L, F, T, DR, RP, PR	[28]
Exhausted coffee waste	32	7.0	110	L, F, DR	[29]
Mercapto-modified bentonite	19	6.17	36.95	L, F, DR	[30]
Zinc oxide nanoparticles	714	5.5	600	L, F	[31]

* L: Langmuir; F: Freundlich; T: Temkin; DR: Dubinin-Radushkevich; RP: Redlich-Peterson; S: Slips; TH: Toth; PR: Radke-Prausnitz; BS: Brouers-Sotolongo

The Langmuir sorption isotherm assumes the monolayer adsorption of particles onto the homogeneous surfaces and could be presented as linear form of equation:

$$\frac{C_e}{q_e} = \frac{1}{q_m K_L} + \frac{C_e}{q_m} \quad (3)$$

where C_e (mg/L) is the equilibrium concentration of Hg in solution, q_e and q_m are the equilibrium and maximum adsorption capacities in mg/g, whereas the Langmuir constant (L/mg) is K_L. The Freundlich sorption isotherm corresponds to multilayer adsorption on energetically heterogeneous surface and has linear form:

$$\log q_e = \log K_F + \frac{1}{n} \log C_e \quad (4)$$

where C_e (mg/L) and q_e (mg/g) is the concentration and adsorption capacity at the equilibrium, n and K_F are Freundlich constants.

The results of the model application are shown in Table 2. As is clear, Langmuir model provides excellent results for both Ag-modified CFAs, indicating a monolayer adsorption. Concerning parent zeolites, while K-ZFA gives acceptable results for Langmuir isotherm, M-ZFA data cannot fit to models but this is expected as the adsorption on this zeolite is negligible with the exception of one point at high liquid phase equilibrium concentration.

Table 2. The parameters of isotherm models for Hg^{2+} adsorption

Sample name	q_{max}^{exp} (mg/g)	Langmuir model			Freundlich model		
		q_e (mg/g)	K_L (L/mg)	R^2	n	K_F	R^2
K-ZFA	3.47	3.14	0.011	0.861	1.58	13.48	0.828
M-ZFA	4.00	4.23	0.001	0.012	2.86	10.85	0.182
Ag-K-ZFA	20.45	20.28	0.037	0.993	2.23	1.66	0.908
Ag-M-ZFA	22.30	22.63	0.103	0.999	3.80	5.35	0.846

3.3. Mechanism studies

The nanocomposite samples were analyzed before and after the interaction with mercury in order to detect the phases in a slow scanning mode and the results are shown in Fig. 6. It could be observed that both post-adsorption samples of nanocomposites contain AgCl (chlorargyrite) attributed to the peaks at 32.23° and 46.25° for K sample and 46.21° and 57.72° for M sample, while the initial Ag NPs has been significantly reduced in amount or almost disappeared, which entails the transformation Ag^{o} to Ag^{+}. As it was proposed in our previous studies on Hg removal [15] the efficient removal might be due to the reduction-oxidation followed by amalgamation reactions. Based on the observed peaks if amalgams are formed the most probable are the Ag_2Hg_3 which gives peaks at 21.77° and 46.16° and Ag_3Hg which gives a peak at 32.29°. However, based on the peaks intensity and position suggests that Hg^{2+} is reduced to Hg^{+} and subsequently reacts with Cl^{-} to form calomel (Hg_2Cl_2). Indeed, relatively intense characteristic of calomel peaks were observed at 21.44°, 28.17° and 43.86° (Ag-K-ZFA) and 21.39°, 28.11° and 43.79° (Ag-M-ZFA).

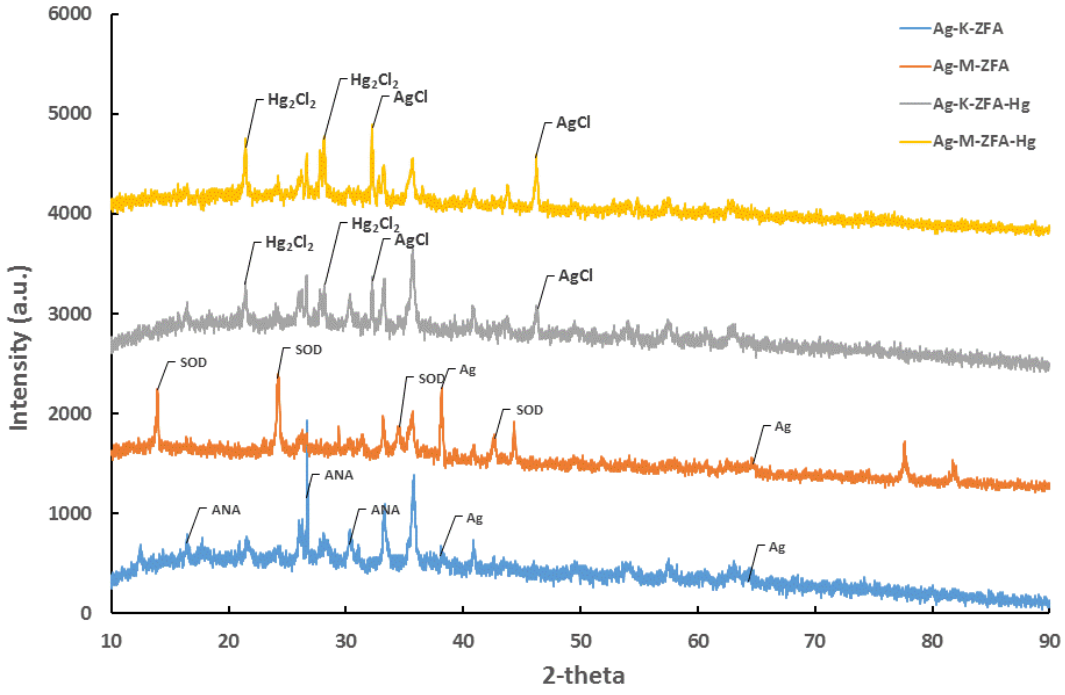

Fig. 6. XRD spectra of Ag-ZFA and Ag-ZFA after interaction with 500ppm Hg^{2+} (SOD: sodalite; ANA; analcime; Ag: silver; AgCl: chlorargyrite; Hg_2Cl_2: calomel)

Taking into account the highest Hg loading values on the Ag samples and subtracting the corresponding Hg adsorbed on parent zeolites the maximum values of the Hg loading attributed to Ag-Hg interaction and molar Hg:Ag ratios are calculated (Table 3).

Table 3. Analysis of equilibrium data.

Sample name	Content (mg/g)		Hg:Ag
	Ag	Hg	
Ag-K-ZFA	22.9	16.7	0.38
Ag-M-ZFA	22.1	19.2	0.45

The Hg:Ag ratio for the formation of calomel is 1:1 however the maximum ratio is 0.38-0.45 and obviously for the rest of isotherm points this value is lower. This shows that although the Hg reduction takes place the major part of Ag is oxidized by the dissolved oxygen in the solution and then reacts with chloride to form AgCl. Another possibility is the formation of amalgams which correspond to Hg:Ag ratio lower than 0.5 [32].

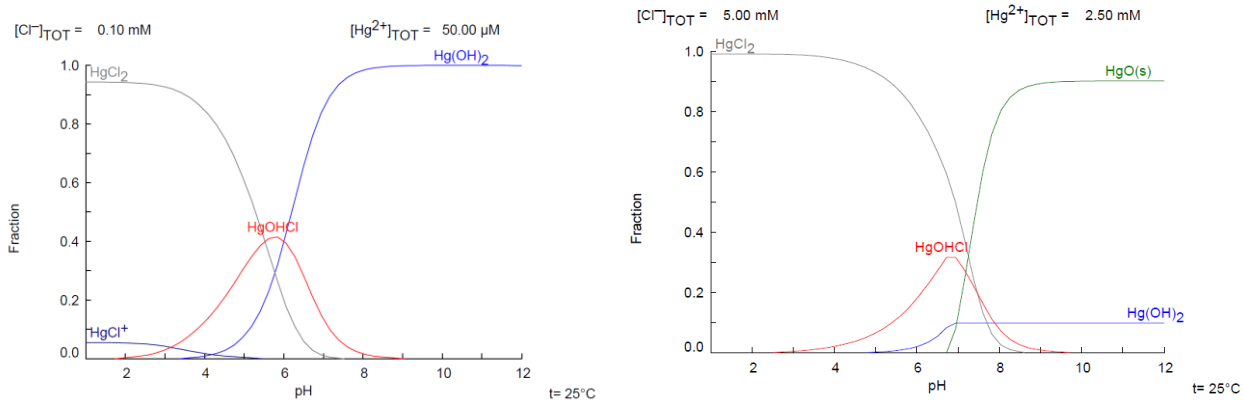

Fig. 7. Speciation of mercury in water with different concentrations.

Any study on the adsorption from water phase should be supported by basic speciation analysis. In Fig. 7 and 8 the mercury speciation in low (10 ppm) and high concentrations (500 ppm). All diagrams were created by using Medusa software. As is clear, mercury exists in the form of neutral

complexes with chloride and thus possible ion exchange with sodium or other cations from the solution is excluded. These complexes should be weak enough for the chloride to be rejected upon the interaction with Ag^o and the reduction of Hg^{2+} to happen. The most probable reactions taking place are as follows:

$$4Ag^o + O_2 \rightarrow 2Ag_2O \quad (5)$$

$$Ag^\circ + Hg^{2+} \rightarrow Hg^+ + Ag^+ \quad (6)$$

$$Ag_2O + 2H^+ \rightarrow 2Ag^+ + H_2O \quad (7)$$

$$Ag^+ + Cl^- \rightarrow AgCl \quad (8)$$

$$Hg^+ + Cl^- \rightarrow HgCl \text{ (or } Hg_2Cl_2) \quad (9)$$

The formation of Ag^+ due to interaction with H^+ contributes to the increase of pH of the solutions. To better understand the Hg-Ag interaction mechanism in Fig. 8 the speciation of Hg in the presence of chloride and silver is presented. The proposed mechanism postulates that Ag^o creates reducing conditions locally on the surface so that the Hg^{2+}-Ag^o interaction to take place and Hg^+ to be produced but the reduction to Hg^o is hindered by the presence of Cl^-.

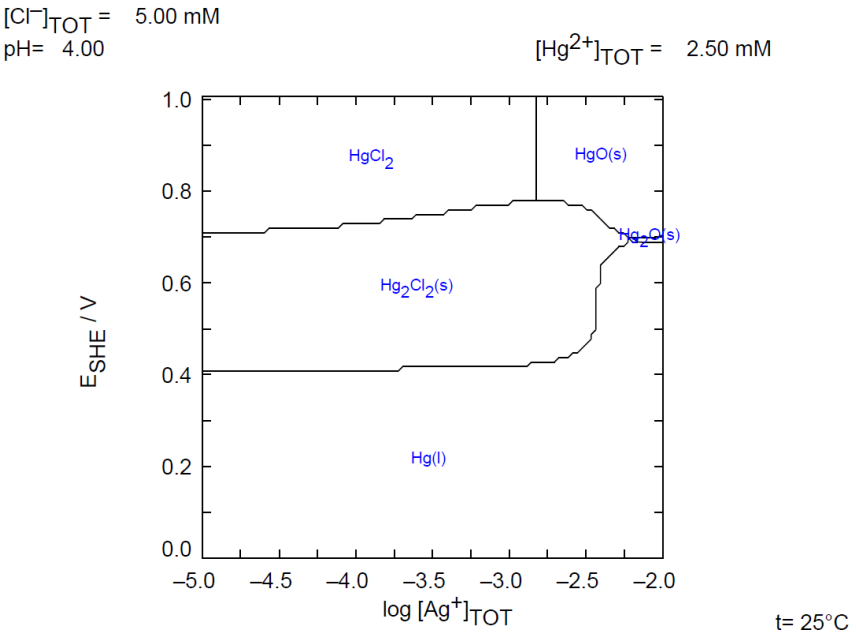

Fig. 8. Speciation of mercury in the presence of chloride and silver.

297 It should be emphasized that AgCl, Hg_2Cl_2 and the potential amalgams are chemically stable,
298 insoluble in water and precipitated on the surface of nanocomposites as all characterizations
299 show. Indeed, the chemical composition by XRF confirms the stability of Ag on the surface after
300 the reaction and the existence of Hg on the surface of the zeolites. The XRF analysis shows Hg
301 content of 28.2 mg/g for Ag-K-ZFA and 40.7 mg/g for Ag-M-ZFA, higher than those calculated from
302 the equilibrium experiments, 20.1 mg/g and 21.9 mg/g, respectively (Table 4). However, it should
303 be noted that the values obtained from XRF are approximate as is a semi-quantitative method.

304
305 **Table 4.** Chemical composition Ag-ZFAs after Hg^{2+} removal, wt.%

Compound	Na_2O	MgO	P_2O_5	K_2O	Al_2O_3	SiO_2	CaO	Fe_2O_3	Ag_2O	HgO
Ag-K-ZFA-Hg	-	0.24	0.22	0.12	14.99	17.59	0.88	58.53	1.83	3.05
Ag-M-ZFA-Hg	-	0.35	4.25	0.17	13.70	21.86	1.84	47.83	1.82	4.40

306

307 Furthermore, the post-adsorption samples of nanocomposites were analyzed on SEM with EDS
308 analysis as shown in Fig. 9 and 10. In both samples EDS analysis shows Hg, Ag and Cl in
309 concentrations around 0.8-1.2% w/w, 2-2.9% w/w and 0.8-0.9% w/w, respectively. The SEM-EDS
310 mapping of Ag-K-ZFA shows Ag and Cl at the same spots of sample that confirms the formation of
311 AgCl. The Hg coexists in several spots with Ag and Cl but due to adsorption is mostly homogeneous
312 distributed on the surface of the zeolite. The SEM-EDS mapping of Ag-M-ZFA is less clear but the
313 conclusions are the same.

314

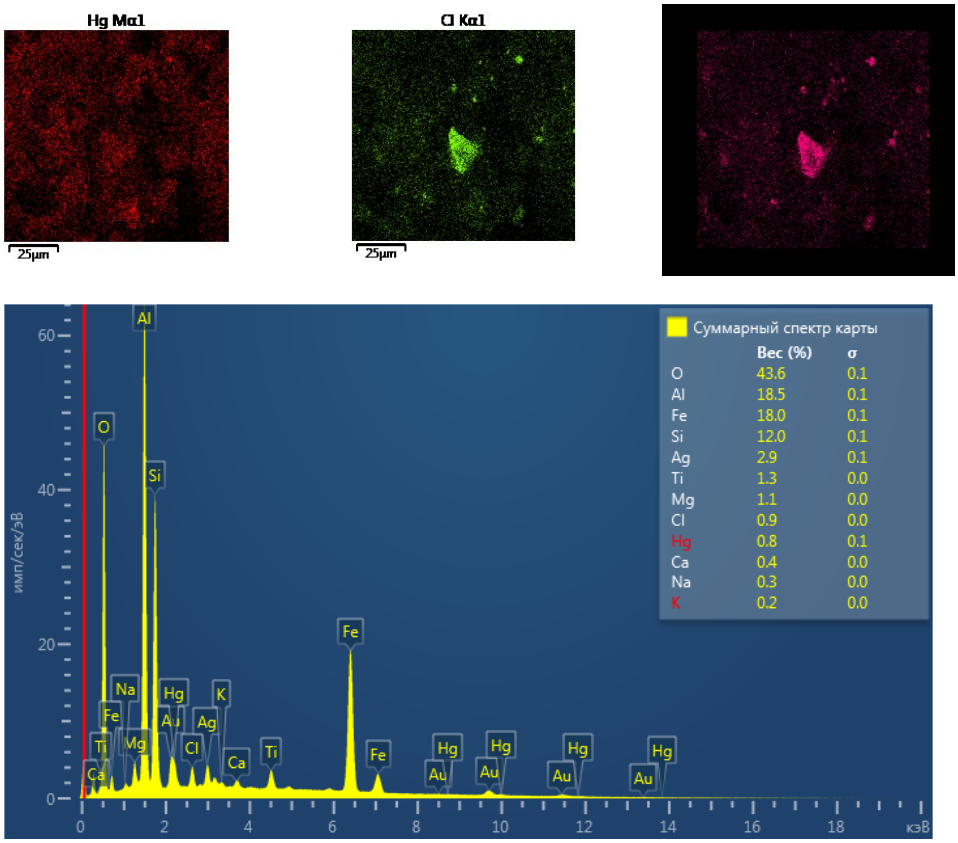

315 **Fig. 9.** SEM mapping of Ag-K-ZFA with Hg (II)

316

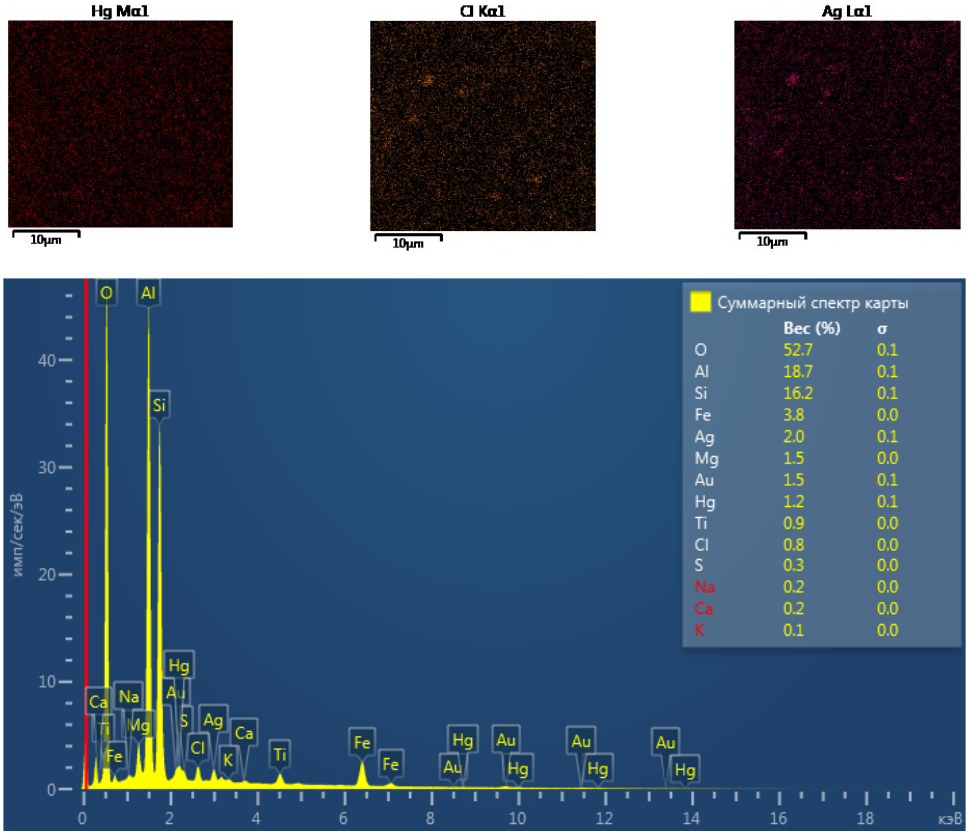

317 **Fig. 10.** SEM mapping of Ag-M-ZFA with Hg (II)

4. Conclusions

In this work, coal fly ash derived zeolites and silver nanocomposites are studied by employing equilibrium and isotherm models. The maximum adsorption capacities of both synthetic zeolites is about 4 mg/g increased by 5 times after the modification with silver nanoparticles to 20.5-22.3 mg/g. Langmuir model describes better than the Freundich model the experimental data for nanocomposites, however they both fail to represent the parent zeolite adsorption. The detailed mechanism studies revealed that Hg^{2+} ions primarily removed by reduction to Hg^{+} followed by formation of calomel (Hg_2Cl_2). There are side reactions as the oxidation of portion of Ag NPs followed by a surface precipitation into AgCl. In addition, there might be amalgam formation reactions but the derived data are inconclusive. The nanocomposites firmly demonstrate the superiority over parent synthetic zeolites and confirm the advantage of Ag NPs impregnation.

Acknowledgements

The authors would like to acknowledge the Nazarbayev University Research Council for funding the project entitled “Noble metals nanocomposites hyper-activity in heterogeneous non-catalytic and catalytic reactions" (Project No. SOE2019012) and Korea Research Fellowship (KRF) program of the National Research Foundation of Korea (Grant No. 2019H1D3A1A01102565) for a postdoctoral fellowship of Dr. Tauanov at Chungnam National University. We would like to acknowledge the Core Facilities Laboratory of Nazarbayev University, particularly research technologists Mrs. Rakhima Shamenova. Mr. Yerzhigit Sugurbekov, and Mrs. Altynai Rysbekova for their provided analysis. We also thank the Oskemen city power plant for providing CFA samples.

Conflicts of interest

There are no conflicts to declare.

References

[1] P. Miretzky, A.F. Cirelli, Hg(II) removal from water by chitosan and chitosan derivatives: A review, J. Hazard. Mater. 167 (2009) 10–23. https://doi.org/https://doi.org/10.1016/j.jhazmat.2009.01.060.

[2] H. Parham, B. Zargar, R. Shiralipour, Fast and efficient removal of mercury from water samples using magnetic iron oxide nanoparticles modified with 2-mercaptobenzothiazole, J. Hazard. Mater. 205–206 (2012) 94–100. https://doi.org/https://doi.org/10.1016/j.jhazmat.2011.12.026.

[3] J.G. Yu, B.Y. Yue, X.W. Wu, Q. Liu, F.P. Jiao, X.Y. Jiang, X.Q. Chen, Removal of mercury by adsorption: a review, Environ. Sci. Pollut. Res. 23 (2016) 5056–5076. https://doi.org/10.1007/s11356-015-5880-x.

[4] V.M. Yau, P.G. Green, C.P. Alaimo, C.K. Yoshida, M. Lutsky, G.C. Windham, G. Delorenze, M. Kharrazi, J.K. Grether, L.A. Croen, Erratum to “Prenatal and neonatal peripheral blood mercury levels and autism spectrum disorders” [Environ. Res. 133 (2014) 294–303], Environ. Res. 134 (2014) 454. https://doi.org/https://doi.org/10.1016/j.envres.2014.09.001.

[5] R. Singh, N. Gautam, A. Mishra, R. Gupta, Heavy metals and living systems: An overview, Indian J. Pharmacol. 43 (2011) 246–253. https://doi.org/10.4103/0253-7613.81505.

[6] H.W. Hsiao, S.M. Ullrich, T.W. Tanton, Burdens of mercury in residents of Temirtau, Kazakhstan. I: Hair mercury concentrations and factors of elevated hair mercury levels, Sci. Total Environ. 409 (2011) 2272–2280. https://doi.org/10.1016/j.scitotenv.2009.12.040.

[7] Y.K. Henneberry, T.E.C. Kraus, J.A. Fleck, D.P. Krabbenhoft, P.M. Bachand, W.R. Horwath, Removal of inorganic mercury and methylmercury from surface waters following coagulation of dissolved organic matter with metal-based salts, Sci. Total Environ. 409 (2011) 631–637. https://doi.org/https://doi.org/10.1016/j.scitotenv.2010.10.030.

[8] H.H. Eriksen, F.X. Perrez, The Minamata Convention: A Comprehensive Response to a Global Problem, Rev. Eur. Comp. Int. Environ. Law. 23 (2014) 195–210. https://doi.org/10.1111/reel.12079.

[9] Margaret A. Coulter, Minamata Convention on Mercury, Int. Leg. Mater. 55 (2016) 582. https://doi.org/10.5305/intelegamate.55.3.0582.

[10] H. Parham, B. Zargar, R. Shiralipour, Fast and efficient removal of mercury from water samples using magnetic iron oxide nanoparticles modified with 2-mercaptobenzothiazole, J. Hazard. Mater. 205–206 (2012) 94–100. https://doi.org/https://doi.org/10.1016/j.jhazmat.2011.12.026.

[11] Z. Tauanov, D. Shah, V. Inglezakis, P.K. Jamwal, Hydrothermal synthesis of zeolite production from coal fly ash: A heuristic approach and its optimization for system identification of conversion, J. Clean. Prod. 182 (2018). https://doi.org/10.1016/j.jclepro.2018.02.047.

[12] N. Koshy, D.N. Singh, Fly ash zeolites for water treatment applications, J. Environ. Chem. Eng. (2016). https://doi.org/10.1016/j.jece.2016.02.002.

[13] M. Attari, S.S. Bukhari, H. Kazemian, S. Rohani, A low-cost adsorbent from coal fly ash for mercury removal from industrial wastewater, J. Environ. Chem. Eng. 5 (2017) 391–399. https://doi.org/10.1016/j.jece.2016.12.014.

[14] D. Czarna, P. Baran, P. Kunecki, R. Panek, R. Żmuda, M. Wdowin, Synthetic zeolites as potential sorbents of mercury from wastewater occurring during wet FGD processes of flue gas, J. Clean. Prod. 172 (2018) 2636–2645. https://doi.org/10.1016/j.jclepro.2017.11.147.

[15] Z. Tauanov, P.E. Tsakiridis, S.V. Mikhalovsky, V.J. Inglezakis, Synthetic coal fly ash-derived zeolites doped with silver nanoparticles for mercury (II) removal from water, J. Environ. Manage. 224 (2018) 164–171. https://doi.org/10.1016/j.jenvman.2018.07.049.

[16] Z. Tauanov, P.E. Tsakiridis, D. Shah, V.J. Inglezakis, Synthetic sodalite doped with silver nanoparticles: Characterization and mercury (II) removal from aqueous solutions, J. Environ. Sci. Heal. - Part A Toxic/Hazardous Subst. Environ. Eng. 0 (2019) 1–9. https://doi.org/10.1080/10934529.2019.1611129.

[17] Z. Tauanov, D. Shah, V. Inglezakis, Silver Nanoparticles Impregnated Zeolites Derived from Coal Fly Ash: Effect of the Silver Loading on Adsorption of Mercury (II), Proceedings. 2 (2018) 647. https://doi.org/10.3390/proceedings2110647.

[18] Z. Tauanov, D. Shah, G. Itskos, V. Inglezakis, Optimized Production of Coal Fly Ash Derived Synthetic Zeolites for Mercury Removal from Wastewater, IOP Conf. Ser. Mater. Sci. Eng. 230 (2017). https://doi.org/10.1088/1757-899X/230/1/012044.

[19] Z. Tauanov, V.J. Inglezakis, Removal of iodide from water using silver nanoparticles-impregnated synthetic zeolites, Sci. Total Environ. (2019). https://doi.org/10.1016/j.scitotenv.2019.05.106.

[20] M.K. Al-Omar, M.A. Alsaadi, T.M. Jassam, S. Akib, M. Ali Hashim, Novel deep eutectic solvent-functionalized carbon nanotubes adsorbent for mercury removal from water, J. Colloid Interface Sci. 497 (2017) 413–421. https://doi.org/10.1016/j.jcis.2017.03.014.

[21] J. Chen, Y. Wang, X. Wei, P. Xu, W. Xu, R. Ni, J. Meng, Magnetic solid-phase extraction for the removal of mercury from water with ternary hydrosulphonyl-based deep eutectic solvent modified magnetic graphene oxide, Talanta. 188 (2018) 454–462. https://doi.org/10.1016/j.talanta.2018.06.016.

[22] S.A. Sajjadi, A. Mohammadzadeh, H.N. Tran, I. Anastopoulos, G.L. Dotto, Z.R. Lopičić, S. Sivamani, A. Rahmani-Sani, A. Ivanets, A. Hosseini-Bandegharaei, Efficient mercury removal from wastewater by pistachio wood wastes-derived activated carbon prepared by chemical activation using a novel activating agent, J. Environ. Manage. 223 (2018) 1001–1009. https://doi.org/10.1016/j.jenvman.2018.06.077.

[23] S. Sobhanardakani, A. Jafari, R. Zandipak, A. Meidanchi, Removal of heavy metal (Hg(II) and Cr(VI)) ions from aqueous solutions using Fe2O3@SiO2 thin films as a novel adsorbent, Process Saf. Environ. Prot. 120 (2018) 348–357. https://doi.org/10.1016/j.psep.2018.10.002.

[24] E.A. Asare, D.K. Essumang, D.K. Dodoo, S. Tagoe, Monitoring & Management Utilization of Bacillus thuringiensis MC28 as a biosorbent for mercury in groundwaters from some selected gold mining communities in the Wassa West District of the Western Region of Ghana, Environ. Nanotechnology, Monit. Manag. 9 (2018) 95–106. https://doi.org/10.1016/j.enmm.2017.12.005.

[25] J.H. Park, J.J. Wang, B. Zhou, J.E.R. Mikhael, R.D. DeLaune, Removing mercury from aqueous solution using sulfurized biochar and associated mechanisms, Environ. Pollut. 244 (2019) 627–635. https://doi.org/10.1016/j.envpol.2018.10.069.

[26] Y. Song, M. Lu, B. Huang, D. Wang, G. Wang, L. Zhou, Decoration of defective MoS2nanosheets with Fe3O4nanoparticles as superior magnetic adsorbent for highly

selective and efficient mercury ions (Hg2+) removal, J. Alloys Compd. 737 (2018) 113–121. https://doi.org/10.1016/j.jallcom.2017.12.087.

[27] Y. Li, W. Li, Q. Liu, H. Meng, Y. Lu, C. Li, Alkynyl carbon materials as novel and efficient sorbents for the adsorption of mercury(II) from wastewater, J. Environ. Sci. (China). 68 (2018) 169–176. https://doi.org/10.1016/j.jes.2016.12.016.

[28] S.A. Vali, M. Baghdadi, M.A. Abdoli, Immobilization of polyaniline nanoparticles on the polyurethane foam derived from waste materials : A porous reactive fixed-bed medium for removal of mercury from contaminated waters, J. Environ. Chem. Eng. 6 (2018) 6612–6622. https://doi.org/10.1016/j.jece.2018.09.042.

[29] N.M. Mora Alvarez, J.M. Pastrana, Y. Lagos, J.J. Lozada, Evaluation of mercury (Hg2+) adsorption capacity using exhausted coffee waste, Sustain. Chem. Pharm. 10 (2018) 60–70. https://doi.org/10.1016/j.scp.2018.09.004.

[30] T. Şahan, F. Erol, Ş. Yılmaz, Mercury(II) adsorption by a novel adsorbent mercapto-modified bentonite using ICP-OES and use of response surface methodology for optimization, Microchem. J. 138 (2018) 360–368. https://doi.org/10.1016/j.microc.2018.01.028.

[31] T. Sheela, Y.A. Nayaka, R. Viswanatha, S. Basavanna, T.G. Venkatesha, Kinetics and thermodynamics studies on the adsorption of Zn (II), Cd (II) and Hg (II) from aqueous solution using zinc oxide nanoparticles, Powder Technol. 217 (2012) 163–170. https://doi.org/10.1016/j.powtec.2011.10.023.

[32] K. V Katok, R.L.D. Whitby, T. Fukuda, T. Maekawa, I. Bezverkhyy, S. V Mikhalovsky, A.B. Cundy, Hyperstoichiometric Interaction Between Silver and Mercury at the Nanoscale, Angew. Chemie Int. Ed. 51 (2012) 2632–2635. https://doi.org/doi:10.1002/anie.201106776.